Joint International Topical Meeting on Mathematics & Computation and Supercomputing in Nuclear Applications (M&C + SNA 2007)
Monterey, California, April 15-19, 2007, on CD-ROM, American Nuclear Society, LaGrange Park, IL (2007)

SUBCELL S_N SWEEPING FOR MESHES WITH REENTRANT CELLS

[†]Frederick N. Gleicher, [*]James S. Warsa, [+]Jim E. Morel and [†]Anil K. Prinja

[†]Department of Chemical and Nuclear Engineering
University of New Mexico
Albuquerque, NM 87131-1344
gleicher@lanl.gov, prinja@unm.edu

[*]P.O. Box 1663, MS D409
Los Alamos National Laboratory
Los Alamos, NM 87545
warsa@lanl.gov

[+]Department of Nuclear Engineering
Texas A&M University
129 Zachry Engineering Center, TAMU 3133
morel@tamu.edu

ABSTRACT

We first motivate a general submesh sweeping technique that avoids the complications associated with sweeping on meshes with reentrant cells. The scattering sources are constructed on a primary mesh, but sweeps are performed on a submesh that underlies the primary mesh. A critical aspect of this approach is the projection of the submesh sweep solution onto the primary mesh for purposes of calculating the scattering sources. We define this projection for standard discontinuous finite-element (DFEM) methods and lumped DFEM methods, and discuss our reasons for making this definition. We give computational results for linear-discontinuous and lumped linear-discontinuous discretizations on a 1-D primary mesh and submesh that demonstrate the efficacy of our approach in terms of accuracy and preservation of the thick diffusion limit for a simple but highly relevant case.

Key Words: discrete-ordinates, finite-element, polygonal and polyhedral meshes, thick diffusion limit

1. INTRODUCTION

The purpose of this work is to present preliminary 1-D theoretical and computational results relating to accuracy and preservation of the thick diffusion limit for a general subcell S_n sweeping technique that is intended to effi ciently accommodate meshes with reentrant cells.

Reentrant cells can greatly complicate the S_n sweeping process. On rectangular meshes, one can always order the angular fluxes for any given direction so that the equations for the characteristic transport operator (streaming plus removal) take the form of a block lower-triangular system with the unknowns in each spatial cell corresponding to a block. This structure ensures that the formal transport operator can be directly inverted via a sweeping or back-substitution process. Thus when such a structure exists, we say that a sweep ordering exists. Cells can be reentrant on both structured and unstructured non-orthogonal meshes. When this occurs, a sweep ordering may not exist, forcing the inversion of the characteristic

operator via an iterative process that can be significantly less efficient than a standard sweep. The absence of reentrant cells guarantees a sweep ordering in 2-D geometries. Although a sweep ordering may not exist on 3-D non-orthogonal meshes with non-reentrant cells, such an occurrence is extremely rare and not of practical importance for most applications. Non-reentrant cells generally occur in two ways. First, almost all general hexahedral meshes contain large numbers of slightly reentrant cells because the cell faces are curved [**?**]. Second, transport is often combined with hydrodynamics in multiphysics simulations such as those associated with inertial confinement fusion. In such calculations, hydrodynamics solution techniques that move the mesh are quite common. The hydrodynamics can easily make cells highly reentrant. Thus there is considerable motivation for finding an efficient way to deal with reentrant cells in S_n calculations.

In principle, an effective strategy for dealing with reentrant cells would be to decompose each cell into a set of non-reentrant subcells. Under the assumption that this decomposition is performed in such a way that a valid global submesh results, one could simply discretize and solve the S_n equations on that submesh. However, this would potentially be expensive in terms of additional memory and CPU time. The memory increase could be completely mitigated by discretizing the scattering sources on the primary or original mesh but discretizing the characteristic operator on the submesh. The sweeps would be carried out on the submesh, but only the scattering sources on the primary mesh would be retained across source iterations. The submesh angular fluxes would be discarded during the sweep process after their contributions to the scattering sources on the primary mesh and the boundary conditions for downwind cells were calculated. In addition, the increase in CPU time may not be as large as it might initially appear to be. For instance, let us assume that we replace a standard hexahedron with a polyhedral-hexahedron by decomposing it into 24 tetrahedra. Such a hexahedron is illustrated in Fig. **??**. Assuming a trilinear-discontinuous finite-element

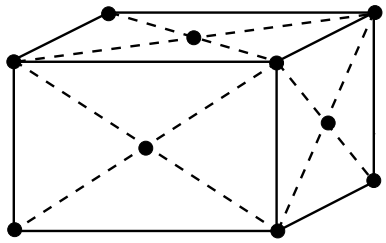

Figure 1. Hexahedron-like polygon composed of 24 tetrahedra.

spatial discretization for the hexahedron results in 8 angular flux unknowns within the cell. Assuming a linear-discontinuous finite-element discretization for each tetrahedron within the polyhedral-hexahedron results in 96 unknowns. An increase of a factor of 12. However, the solution within each tetrahedron is obtained independently, requiring a direct 4×4 matrix solution. The trilinear solution for the entire polyhedron requires a direct 8×8 matrix solution. Assuming that a direct solution requires $O(N^3)$ operations, we find that the submesh calculation requires on the order of 1536 operations while the primary mesh calculation requires on the order of 512 operations. Thus the submesh sweep requires about three time more operations than the primary mesh sweep even though there are 12 times as many unknowns on the submesh. This is far from a rigorous analysis, but it makes an important point. There are further advantages to this approach on general polyhedral meshes where an underlying tetrahedral mesh can mitigate the load balancing problems in parallel calculations arising from polyhedrons with different numbers of faces.

Two questions naturally arise when considering the subcell sweeping approach that we have outlined. The first is to determine the level of accuracy that one can expect, and the second is to determine the

requirements for preserving the thick diffusion limit. To address these questions in a totally general context is too large a task. Instead, we restrict consideration to general polygonal meshes in 2-D and general polyhedral meshes in 3-D. We further assume discontinuous piecewise-linear basis functions for such cells as defined by Stone and Adams [**?**]. Such cells are naturally decomposed into triangles in 2-D and tetrahedra in 3-D. The basis function dependence is linear within each subcell and continuous across all boundaries internal to the polyhedral cell, and discontinuous across the outer boundaries of the cell. We will assume a linear-discontinuous finite-element discretization of the characteristic equation on each subcell and construct the scattering sources on the primary cell using the piecewise-linear basis functions. A critical point for purposes of analysis is that the space of finite-element functions defined on the primary (polygonal/polyhedral) mesh is a subspace of the space of finite-element functions defined on the subcell (triangular/tetrahedral) mesh. For simplicity we henceforth refer only to polyhedral meshes and tetrahedral subcell meshes, but it should be recognized that all statements will have an analog for polygonal cells and triangular subcell meshes.

2 DEFINING THE PROJECTION

A fundamental task associated with this method is to define the projection that maps the subcell sweep solutions to the primary mesh for purposes of constructing the scattering sources. All finite-element methods are actually defined in terms of such a projection. For instance, Galerkin finite-element solutions are defined by the requirement that the projection of the residual onto the trial space be the zero function. If we were to map an arbitrary function to the trial space using a standard Galerkin projection, it would simply take the form of an integral least-squares fit. In particular, consider a finite-element space of functions having basis functions $\{B_n(\overrightarrow{r})\}_{n=1}^{N}$ defined on some spatial domain $\mathcal{D}$. Further consider an arbitrary integrable function $f(\overrightarrow{r})$ defined over the same domain. The Galerkin projection of f onto the finite-element space can be represented as follows:

$$\tilde{f}(\overrightarrow{r}) = \sum_{n=1}^{N} \tilde{f}_n B_n(\overrightarrow{r}) \quad , \tag{1}$$

where the expansion coefficients are chosen to minimize the following functional:

$$\Gamma = \int_{\mathcal{D}} \left(f(\overrightarrow{r}) - \tilde{f}(\overrightarrow{r}) \right)^2 dV \quad . \tag{2}$$

This is equivalent to requiring that $f - \tilde{f}$ be orthogonal to the trial space:

$$\int_{\mathcal{D}} f(\overrightarrow{r}) B_n(\overrightarrow{r})\, dV = \int_{\mathcal{D}} \tilde{f}(\overrightarrow{r}) B_n(\overrightarrow{r})\, dV \quad , \quad n = 1, N. \tag{3}$$

We propose to use this least-squares projection in our subcell sweeping technique when the finite-element sweep equations on the subcell mesh are not lumped. When they are lumped, we must modify the projection. It is not difficult to show that standard mass-matrix lumping is equivalent to using quadrature to perform the integrals in Eq. (**??**). In particular, Eq. (**??**) becomes

$$\sum_{k=1}^{N} f(\overrightarrow{r}_k) B_n(\overrightarrow{r}_k) V_k = \sum_{k=1}^{N} \tilde{f}(\overrightarrow{r}_k) B_n(\overrightarrow{r}_k) V_k, \quad n = 1, N. \tag{4}$$

where the quadrature weights are given by

$$V_k = \int_{\mathcal{D}} B_k(\overrightarrow{r})\, dV \quad . \tag{5}$$

It is important to recognize that in our application, the basis functions for the projection are defined on the polyhedral mesh, but the lumping is occurring on the tetrahedral mesh. Thus for our purposes, Eqs. (**??**) and (**??**) respectively become

$$\sum_{k=1}^{N_t} f(\vec{r}_k) B_{n,p}(\vec{r}_k) V_k = \sum_{k=1}^{N_t} \tilde{f}(\vec{r}_k) B_{n,p}(\vec{r}_k) V_k, \quad n = 1, N_p, \tag{6}$$

and

$$V_k = \int_{\mathcal{D}} B_{k,t}(\vec{r})\, dV \quad . \tag{7}$$

where f denotes the tetrahedral-mesh solution, $\tilde{f}$ denotes the polyhedral mesh solution used to construct the scattering source, $B_{n,p}$ denotes the polyhedral-cell basis function associated with vertex n, $B_{k,t}$ denotes the tetrahedral-mesh subcell basis function associated with vertex k, N_p denotes the number of vertices on the polyhedral cell, and N_t denotes the number of vertices on the tetrahedral subcell mesh. It is also important to note that the basis function associated with a vertex on the tetrahedral subcell mesh that appears in Eqs. (**??**) and (**??**) is obtained by summing all of the fundamental basis functions that share that vertex.

3 ACCURACY AND THE DIFFUSION LIMIT

We expect to obtain second-order accuracy for the polyhedral-mesh solution using this projection because the standard piecewise-linear discontinuous finite-element approximation applied on the polyhedral mesh is second-order accurate and our method simply replaces a sweep solution on the polyhedral mesh with a more accurate sweep solution on the tetrahedral subcell mesh. We would also expect the thick diffusion limit to be preserved because the finite-element approximation applied on the polyhedral mesh preserves this limit. However, the diffusion limit is a sensitive limit, so some analysis is desirable. To perform our analysis, we consider the simplest possible arrangement of primary mesh and subcell mesh: a 1-D primary mesh in 1-D slab geometry with each primary cell (playing the role of the polyhedral mesh) decomposed into two equal subcells (playing the role of the tetrahedral subcell mesh). The corresponding unknowns are illustrated in Fig. **??**. A linear discontinuous discretization is used on the subcell mesh and a

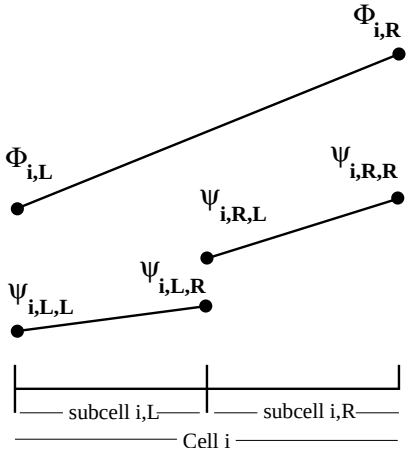

Figure 2. Linear-discontinuous fine-mesh and coarse-mesh unknowns.

linear-discontinuous representation is used on the primary mesh. Note that the angular flux, ψ, exists on the subcell mesh, while the scalar flux used in the scattering source, Φ, exists on the primary mesh. Further note that $\Phi_{i,L}$ and $\Phi_{i,R}$ are defi ned in terms of the subcell-mesh scalar fluxes, $\phi_{i,L,L}$, $\phi_{i,L,R}$, $\phi_{i,R,L}$, and $\phi_{i,R,R}$, using the least-squares projections previously defi ned for the mass-matrix lumped and unlumped discretizations. We have performed an asymptotic analysis for the thick-diffusion limit indicating that our unlumped subcell sweeping technique yields the same diffusion limit equations to leading order as the unlumped linear-discontinuous discretization applied on the primary mesh. This is an excellent result. Our analysis also indicates that the our lumped subcell sweeping technique yields diffusion limit equations to leading order that can be viewed as a linear combination of those obtained by applying the unlumped and lumped linear-discontinuous discretizations to the primary mesh. This is also a very good result.

4 COMPUTATIONAL RESULTS

We now present two sets of computational experiments. One set shows the order of accuracy in the transport limit and the other illustrates that the methods preserve the diffusion limit. The subcell sweeping method for both lumped and unlumped discretization using two subcells per mesh element is compared against the standard LD discretization on the primary mesh.

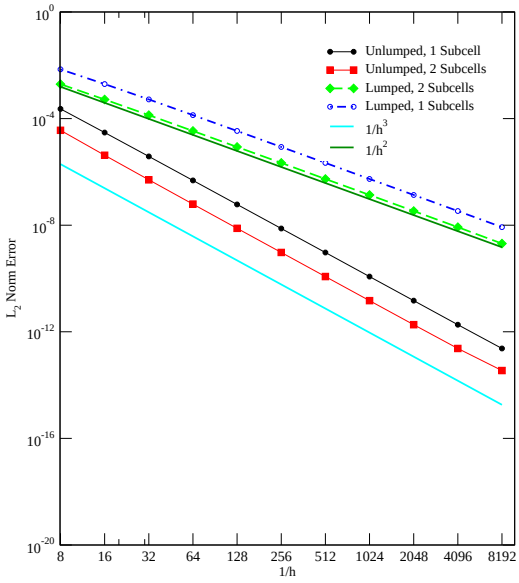

Figure 3. Truncation error order of accuracy in the transport limit.

In Fig. 3 we show the discrete L_2 error norms of the (projected) primary mesh cell-average scalar fluxes for a slab thickness of 1 cm, $\sigma_t = 1$ cm^{-1}, a scattering ratio of $c = 0.95$, and an isotropic distributed source of unit strength, measured against an S_4 analytic solution [**?**]. This set of computations shows that in the transport limit, the unlumped subcell sweep method is third order accurate and the lumped method is second order accurate, preserving the same order of accuracy as the standard LD discretizations on the primary mesh.

In Fig. 4 we show the scalar flux distributions for the same scattering ratio, angular quadrature, and source distribution as in Fig. 3. In Fig. 4 we set the number of coarse mesh cells to 256.

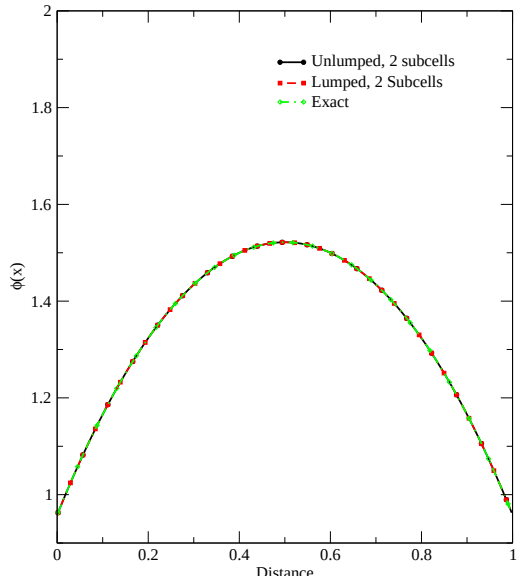

Figure 4. Truncation error order of accuracy in the transport limit.

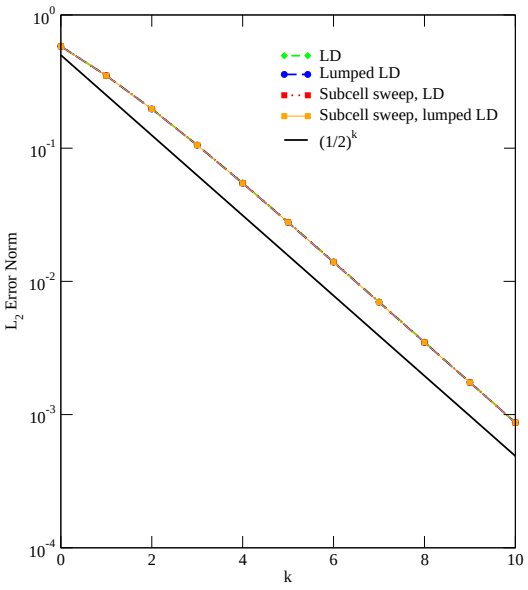

Figure 5. Order of accuracy in the diffusion limit.

In Fig. 5 we show the discrete L_2 error between the projected cell-average scalar fluxes and the scalar fluxes computed using a continuous fi nite element diffusion equation discretization (with mass matrix lumping in the lumped case). The angular quadrature for this case is S_8, and the slab is 1 cm thick. The

problem is scaled to be increasingly thick and diffusive in the asymptotic parameter $\epsilon \to 0$ according to

$$\begin{aligned}
\sigma_t &\longrightarrow \frac{\sigma_{t,0}}{\epsilon} \\
\sigma_a &\longrightarrow \epsilon\sigma_{a,0} \\
\sigma_s &\longrightarrow \frac{\sigma_{t,0}}{\epsilon} - \epsilon\sigma_{a,0} \\
q &\longrightarrow \epsilon q_0
\end{aligned}$$

with the initial problem parameters

$$\begin{aligned}
\sigma_{t,0} &= 1\ cm^{-1} \\
\sigma_{a,0} &= 0.05\ cm^{-1} \\
q_0 &= 1\ cm^{-3}\ s^{-1}
\end{aligned}$$

and where q_0 is an isotropic distributed source. We let let $\epsilon = 1/2^k$ and plot the error as a function of k. The error decreases with increasing k, showing the expected $\mathcal{O}(\epsilon)$ trend and confi rming that the all the methods have the diffusion limit to leading order.

ACKNOWLEDGMENTS

We acknowledge several invaluable conversations with Professor Marvin Adams of Texas A&M University regarding piecewise-linear polyhedral basis functions and associated fi nite-element techniques. This work was supported by Los Alamos National Laboratory, operated for the US DOE by Los Alamos National Security, LLC, under contract No. DE–AC52–06NA25396.

REFERENCES

[1] T. A. Wareing, J. M. McGhee, J. E. Morel, and S. D. Pautz, "Discontinuous Finite Element Sn Methods on 3-D Unstructured Grids," *Nuclear Science and Engineering*, **138**, 256-268 (2001).

[2] Hiromi G. Stone and Marvin L. Adams, "New Spatial Discretization Methods for Transport on Unstructured Grids," *Mathematics, Computation, Reactor Physics, and Nuclear and Biological Applications*, Palais des Papes, Avignon, France, September 12-15, 2005, on CD-ROM, American Nuclear Society, Lagrange Park, IL (2005).

[3] J. S. Warsa, "Analytical S_N solutions in heterogeneous slabs using symbolic algebra computer programs," *Annals of Nuclear Energy*, **29**, 851-874 (2002).